PCCP

Binding and activation of ethylene on Tungsten carbide and Platinum surfaces

Journal:	*Physical Chemistry Chemical Physics*
Manuscript ID	CP-ART-06-2019-003214.R1
Article Type:	Paper
Date Submitted by the Author:	09-Jul-2019
Complete List of Authors:	Jimenez-Orozco, Carlos; University of Medellin, Faculty of Basic Sciences Florez, Elizabeth; University of Medellin, Faculty of Basic Sciences Montoya, Alejandro; University of Sydney, Chemical & Biomolecular Engineering Rodriguez, Jose; Brookhaven National Laboratory, Chemistry Department

Binding and activation of ethylene on Tungsten carbide and Platinum surfaces

Carlos Jimenez-Orozco,[a*] Elizabeth Florez,[a] Alejandro Montoya,[b] and Jose A. Rodriguez[c*]

[a] Universidad de Medellín, Facultad de Ciencias Básicas, Carrera 87 No 30-65, Medellín, Colombia

[b] University of Sydney, School of Chemical and Biomolecular Engineering, Sydney, NSW 2006, Australia

[c] Brookhaven National Laboratory, Chemistry Department, Upton, New York 11973, United States

ABSTRACT

Density functional calculations were used to evaluate the ability of cubic and hexagonal phases of tungsten carbide to bind ethylene, as a model compound of unsaturated hydrocarbons, since its adsorption is the first step in important catalytic processes. The calculations give the following trend in stability: α-WC(0001)-C > α-WC(0001)-W > Pt(111) > γ-WC(001), with the binding energy varying in the range of -0.72 to -2.91 eV. The sub-surface layers play a crucial role in the binding, favoring a charge reorganization at extended ranges (above 6 Å) from bulk towards the surface, however, the electronic structure of the surface was modified only in the topmost layer. The surface sites for geometric C_2H_4 activation were identified, leading to a surface distortion due to an upwards shifting of surface atoms in the range 0.13–0.61 Å was observed in Pt(111), α-WC(0001)-C, and γ-WC(001), with distortion energies of 0.13, 0.15 and 0.61 eV, respectively. The activation of C_2H_4 on tungsten carbides was compared with other transition metal carbide surfaces, which leads to a general classification of the elongation

of carbon-carbon bond into a set of only three groups. If the interest is to activate ethylene C=C bond, the surface sites and the binding modes should be those of the *groups II* and *III*. The infrared spectra show mainly four useful signals as a fingerprint to support and complement future experiments. The results of this work indicate that the α-WC-W surface could be directly responsible for the catalytic performance, while the binding of olefins on α-WC-C could cause surface poisoning. The metastable γ-WC(001) surface could be a promising system as compared to the known α-WC(0001) surface, but challenges arise regarding its synthesis, stability and catalytic performance. These results pave the way to address further experimental and theoretical studies focused on the hydrogenation of ethylene and more complex unsaturated hydrocarbons.

1. Introduction

Heterogeneous catalysis plays a crucial role in both industry and academia. Particularly, catalyzed hydrogenation reactions of unsaturated hydrocarbons are essencial in the production of several polymers, solvents, food wrap, and clean fuels. The most used catalysts for the hydrogenation of unsaturated hydrocarbons come Pt-group metals. There are some limitations in their long term use due to their apparent poisoning in streams containing sulfur, which is problematic in the current petrochemical industry. Additionally, the production and commercialization of Pt-group metals are expensive, as they have a low abundance in the Earth crust.

For the reasons mentioned above, it is essencial, within the framework of heterogeneous catalysis, to search for materials alternative to the Pt-group metals but conserving a similar catalytic activity and selectivity. Levy and Boudart reported a landmark work[1] regarding the use of tungsten carbide (WC) as a catalyst with a Pt-like behavior. There has been a remarkable increase in the number of works about the use of tungsten and other transition metal carbides (TMCs) with catalytic potential for several hydrogenation reactions.[2,3,12,4–11] However, there is still a lack in the understanding of interactions between the carbide and olefins, which involves even more challenging study to the known ones to date. There are challenges to improve the catalytic activity, selectivity to a desired product and stability under several conditions (causes of deactivation) since the deposition of adsorbates and its decomposed products on surfaces has been observed,[7,9,13–17] particularly in the hydrogenation of unsaturated hydrocarbons.

A basic understanding about interactions at the atomic level is required for the surface-adsorbate system since the knowledge built-on this basis could help to improve the design and performance of TMCs-based catalysts; for this purpose, a model adsorbate should be

considered. In this way, ethylene (C_2H_4) has been widely used as a probe molecule to understand the chemistry associated with olefin hydrogenation processes, leading to a more in-depth knowledge about solid-gas interactions and the concomitant improvement in catalyst design.

We carry out a systematic study, by coming back to the original idea of Levy & Boudart, i.e. using tungsten carbide (WC) as an alternative catalyst to platinum, for hydrogenation of ethylene as a model compound of olefins, where binding plays a vital role.

The first step in ethylene hydrogenation is *adsorption*, where the binding of C_2H_4 on surfaces of solids should be understood in detail as it is the basis for carrying out hydrogenation reactions. Additionally, the study of C_2H_4 adsorption could account for issues regarding hydrocarbon deposition on TMCs surfaces. The transformation of ethylene into its hydrogenated product (ethane) necessarily involves a geometric activation of C_2H_4, i.e. an elongation of C–C bond length and a change in hybridization from sp^2 to sp^3-like. Therefore, the surface sites involved in the binding and the extent of the activation should be identified, together with the characterization of the adsorbate and surface geometric and electronic properties.

Tungsten carbides (WC, W/C=1) have several crystal structures,[18] but the most stable and reported one is the hexagonal system according to its diagram phases, hence, the hexagonal system is used in this work. Even though the cubic system is less stable than the hexagonal one,[19] it is a metastable phase that can be formed,[20] which eventually could be transformed into the hexagonal system. Therefore, the metastable cubic phase is also considered to analyze its potential in the binding and activation of ethylene, since no reports are known about it. The notation of the crystal systems could be confusing since there is not a standard one, but in this work we follow the nomenclature previously reported by Kurlov and Gusev,[18] where cubic and hexagonal systems are denoted as γ-WC and α-WC, respectively. The γ-WC has a rock salt-like structure, which leads to simple low Miller index surfaces, where the (001) has been reported[21] in a previous study. For the case of the α-WC system, the most stable surface is the (0001), for which several works have been reported.[22–29] The α-WC(0001) exposes charged surfaces which can be C or W terminated, hence, both surfaces are analyzed; for the sake of simplicity, these surfaces are labeled as α-WC-C and WC-W, respectively.

Our purpose is to analyze the binding of C_2H_4 and the relevant surface sites involved in γ-WC(001), α-WC-C, and α-WC-W systems, together with the analysis of changes in both geometry and electronic structure of adsorbate and tungsten carbide surfaces. Additionally, we attempt to establish which system (α-WC-C or α-WC-W) has the better performance for C_2H_4 binding and activation under a heterogeneous catalyst scheme, taken the known Pt(111) surface as a reference system. Moreover, the potential of the metastable system γ-WC(001) for ethylene binding and activation is also analyzed.

This work is divided as follows: First, several adsorption modes are evaluated on γ-WC(001), α-WC-C, and α-WC-W surfaces. Second, for the most stable structures, the geometric activation of ethylene is investigated and compared to other TMCs and Pt(111) surfaces. At this point, surface relaxation is discussed. Third, infrared spectra for adsorbed ethylene is discussed, serving as a bridge from modelling and further experiments and theoretical studies. Finally, the role of sub-surface layers in the binding of ethylene is analyzed, together with changes in the electronic structure from the topmost surface layer into the bulk structure.

2. Methodology and Computational Details

Model

The bulk structures of platinum, γ-WC and α-WC were relaxed, obtaining cell parameters (a,b,c) close to the experimental values,[21] with relative errors ≤ 2 % (a=b=c=2%, a=b=c=0.3% and a=b=0.5, c=0.3%, respectively). Then, the surfaces were created following the slab approximation, including a vacuum > 15Å to avoid interactions with the neighbor slab in the direction perpendicular to the surface. Test studies were carried out for vacuum > 30 Å, but the results are the same as for vacuum > 15 Å with a lower computational cost for the latter case. A constant 6% surface coverage of ethylene was used in all the cases; then, the supercell size for Pt(111) and α-WC(0001) is p(4x4) in both cases, while for γ-WC(001) a p(2x2) size was used. Tests analysis were carried out to establish the required number of layers to describe the analyzed systems better. Particularly for the γ-WC(001) surface, the adsorption energies for four-, six-, and eight-layers slab were -0.78 eV, -0.37 eV and -0.36 eV, respectively, therefore, 6 layers are required to describe the slab size better; a similar behavior was observed for adsorption on α-WC(0001) surface (see Table S1 in the Supplementary Information). Additionally, tests studies let us establish that the two outermost layers of the slabs for the γ-WC(001) and α-WC(0001) surfaces should be relaxed, where the four inner layers were fixed to represent the bulk systems. For comparison purposes, a 6-layer slab was also used for the Pt(111) surface.

The binding of ethylene on the γ-WC(001) and α-WC(0001) surfaces was carried out systematically, considering all the surface sites and orientations of the adsorbate. For details about the geometry of our initial adsorption structures and the nomenclature used in this work, please refer to our previous works.[30,31]

Computational details

Calculations within the framework of periodic density functional theory were performed using the VASP code,[32] with the PBE-GGA functional. The electronic density of the valence electrons was expanded in a plane-wave basis set where the associated kinetic energy does not exceed 400 eV cutoff energy. The description of the effect caused by the core electrons in the valence region is described by the projected augmented wave (PAW) method of Blöch, as implemented by Kresse and Joubert.[33] A **k**-points grids were used for the numeral integration of the Brillouin zone, according to the Monkhorst-Pack

scheme. [34] Test studies let us establish the cut-off and **k**-points grids for the surfaces. For the bulk, a mesh of 5x5x5 was used, while a mesh of 5x5x1 was utilized to represent α-WC(0001) and γ-WC(001) surfaces, which has a **k**-spacing of 0.14 $Å^{-1}$ in both cases for the x,y plane of the reciprocal space. For the case of Pt(111) surface, a 3x3x1 mesh was used (**k**-spacing of 0.21 $Å^{-1}$). In all the cases, the meshes are **Γ**-centered. The establishment of the cut off energy and **k**-points mesh in every system is sketched in Fig. S1 and S2. The convergence criteria in subsequent iterations are variations in interatomic forces lower than 0.01 eV/Å, and changes in total energy lower than 10^{-6} eV. A counterdipole was located in the direction perpendicular to the surface to avoid dipole coupling between repeated slabs. For platinum systems, spin-polarized calculations were carried out, but tests studies indicate that for the carbides spin-polarized calculations lead to the same results as for non-spin polarized; then, non-spin polarized calculations are carried out for tungsten carbide systems.

For the binding of ethylene, the adsorption energy (E_{ads}) was calculated as shown in Eq. 1.

$$E_{ads} = E_{slab + ethylene} - E_{slab} - E_{ethylene} \quad (1)$$

In Eq. 1, $E_{slab + ethylene}$ is the energy of the adsorbed ethylene on the clean surface, E_{slab} is the energy of the clean surface, while $E_{ethylene}$ is the energy of the isolated C_2H_4 in an asymmetric box of 13x14x15 Å which was optimized at the **Γ** point. The contribution of dispersion to the adsorption energies was accounted for using the Grimme's D3 where the dispersion term is added to the GGA energy. For the $E_{slab + ethylene}$ and $E_{free\_ethylene}$ systems, the final energy values include the Zero Point Energy (ZPE) term (see Eq. 2). For this purpose, the vibrational frequencies (ν_i) of the adsorbed ethylene (or ν_j of the free C_2H_4) were established using a diagonalization of the Hessian matrix with small finite displacement of analytical gradients by 0.01 Å to ensure that movements are within the harmonic limit. Then, the ZPE term can be computed, considering also the normal vibration modes (*N* or *M*), the Plank constant (*h*) and the relevant units (*c*) in equation (2). Therefore, the vibrational modes of adsorbed ethylene can be used to build an infrared spectrum to complement the characterization of the C_2H_4 binding on surfaces.

$$E_{ZPE,\,included} = \left[E_{slab + ethylene} + \left(\sum_{i}^{N} \frac{1}{2} \times c \times h\nu_i\right)_{ads\_ethylene}\right] - E_{slab} - \left(E_{free\_ethylene} + \sum_{j \neq i}^{M} \frac{1}{2} \times c \times h\nu_j\right)_{free\_ethylene} \quad (2)$$

The electron density changes after ethylene adsorption were analysed utilizing the Charge Density Difference (CDD, named as $\Delta\rho$) schemes, calculated as shown in Eq. 3.

$$\Delta\rho = \rho_{E-S} - \rho_S - \rho_E \quad (3)$$

In Eq. 3, ρ_{E_S} is the electron density of the system *slab+ethylene*, ρ_S is that of the surface in the adsorption geometry but without considering the adsorbate, and ρ_E is that of the ethylene in the adsorption geometry but without the presence of the surface.

For the characterization of the Projected Density of States (PDOS), a mesh of 11x11x1 was considered in all the cases. The same applies to the generations of the CDD plots, Electron Localization Functions (ELF), and the determination of Bader charges. Additionally, for the establishment of the Bader Charges, a vacuum > 30 Å was used for all the studied systems, using the code developed by Henkelman and co-workers.[35–37]

The results of this work are contrasted with our previous findings.[30,31] Even though those reports were obtained using the CASTEP code, the trends and general conclusions are the same as obtained with the VASP code as discussed before.[31] Therefore, the comparison of the results of this work can be directly compared to our previous data, both geometries and energies.

3. Results and Discussion

3.1. Adsorption of C_2H_4 on γ-WC(001) and α-WC(0001) surfaces

Several possibilities for the binding on ethylene were evaluated as there are different surface sites in every case. The ELF charts (see Fig. S3 in the Supplementary Information) serve as a guide to locate the adsorbate on the surfaces.

Among the set of initial evaluated adsorption modes, some structures converged to the same geometry, which is summarized in Tables S2 and S3 (see Supplementary Information). For the case of α-WC-C and α-WC-W, only three structures were found in every surface, while eleven different geometries were obtained on the γ-WC(001) system. It is indicative that on the last surface there is a higher diversity of surface sites, as compared to the α-WC-C and α-WC-W surfaces. The most stable adsorption energy in every surface is shown in Table 1, while the respective geometries are reported in Fig. 1. As there is still a lack of experimental information regarding adsorption energies, the range DFT to DFT+vdW could provide a region where experimental values can be located in. The obtained general trends using DFT or DFT+vdW are equivalent. Hence most analyses are considered using one of them, otherwise specified DFT+vdW is used.

The ELF in Fig. S3a indicates that the γ-WC(001) surface is a non-charged surface, where the location of regions with high and low electron density belongs to those of the C and W atoms, respectively. On the contrary, the ELF for α-WC-C and α-WC-W indicates that they are charged surfaces, where the negative charge is exposed to a greater extent in the topmost layer of the α-WC-C surface. In both α-WC-C and α-WC-W atoms, the layers of W have less electron density, while the layers of C atoms have higher electron density coming from the other W layers. Therefore, the arrangement of alternately positive and negative layers favors the strong adsorption of adsorbates on α-WC(0001), since a charge reorganization (perpendicular to the *z*-direction of the slab) from the bulk of the system into the surface layer could be possible. However, this kind of charge reorganization in

the γ-WC(001) system could be diminished, as there is a mixture of C and W atoms in the *x,y* direction of the slab in every layer, decreasing the effect of charge exodus in the direction parallel to the *z*-axis of the slab.

On the γ-WC(001) and α-WC-C surfaces, a $C_{surface}$–$C_{ethylene}$ bond is formed (i.e. di-σ-CC mode), which is in agreement with the location of negative charges in $C_{surface}$ atoms as shown in the ELF charts (Fig. S3). In the binding of ethylene on the α-WC-W surface (Fig. 1d), the $C_{ethylene}$ atoms are located atop hollow surface sites which are above $C_{sub-surface}$ sites, where the charge coming from the sub-surface C atoms of the α-WC-W surface leads to an increase in the electron density in the hollows of the W surface. Hence, the carbon atoms or the region in between the C=C bond of the ethylene molecule are located atop hollow sites of the α-WC-W surface (see Table S3). Therefore, the sub-surface C layer plays a crucial role in the binding on this substrate.

The binding on two tungsten carbide surfaces (γ-WC(001) and α-WC-C) is favored by using two surface carbon atoms, which has a similarity in terms of binding mode on TiC(001) as previously reported.[30] On the contrary, the binding on γ-WC(001) and α-WC-C has a different behavior as compared to other surfaces[30] like δ-MoC(001), ZrC(001), and β-Mo_2C-C,[31] where only one surface atom is directly involved in the binding, particularly Mo and Zr atoms in their respective carbides. The binding behavior of C_2H_4 on TMCs with the similar surface geometric arrangement, i.e. from a cubic rock-salt bulk and the same supercell size and a (001) surface, follows the trend in terms of DFT adsorption energy (in *eV* units):

γ-WC(001) (-0.72) > δ-MoC(001) (-0.53) > TiC(001) (-0.45) >> ZrC(001) (-0.12)

For the case of tungsten carbide surfaces, the adsorption energy extent for the most stable binding structures of ethylene follows the trend (both DFT and DFT+vdW):

α-WC-C >>> α-WC-W > Pt(111) > γ-WC(001)

Among the systems mentioned above, only in γ-WC(001) and TiC(001) systems, the ethylene is activated in the same adsorption mode (i.e. di-σ-CC), where the extent of the $C_{ethylene}$-$C_{ethylene}$ bond length elongation is equivalent (from 1.33 Å to 1.60 Å in both cases). Therefore, the C_2H_4 adsorption on γ-WC(001) has advantages over δ-MoC(001) and ZrC(001) surfaces, as the interaction is stronger together with the elongation of the C=C bond length. For comparison, the binding on Pt(111) surface is stronger (-1.23 eV) than the cases shown above, which indicates that an ensemble effect in carbides favors a decrease in the binding energy for the systems shown above. Overall, the γ-WC(001) and TiC(001) could have similar behavior in terms of an initial C_2H_4 geometry modification

in further analysis regarding hydrogenation reactions; however, these aspects are beyond the scope of this work and could be a matter of future work.

Ethylene binding to the carbides of the group 6 in the Periodic Table, i.e. molybdenum and tungsten carbides, has several differences in terms of geometry and energy. The reported surfaces for molybdenum carbides for ethylene adsorption are δ-MoC(001)[30] and β-Mo_2C(100),[31] where the last system has charged C (β-Mo_2C-C) and Mo terminations (β-Mo_2C-Mo). The similar (001) surfaces built from a rock salt-like structure were contrasted above. On the other hand, β-Mo_2C(100) and α-WC(0001) has different structures since they proceed from different bulk crystal systems, viz. orthorhombic and hexagonal, respectively; however, in both cases, there are charged C- and M-terminations. Nevertheless, the geometry of both systems is different, particularly the distance $C_{surface}$–$C_{surface}$ in the C-termination is larger in β-Mo_2C-C (3.08–6.04 Å) than in α-WC-C (2.93 Å); additionally, the packing of C and M atoms is different in both systems. Therefore, the binding is non-comparable directly for the β-Mo_2C-C and α-WC-C systems in terms of geometry. However, general trends can be achieved: 1) for C-termination, the binding is stronger on α-WC-C (-2.91 eV) than on β-Mo_2C-C (-1.87 eV); 2) the adsorption is weaker on α-WC-W (-1.68 eV) than on β-Mo_2C-Mo (-4.23 eV). Therefore, there is not a clear trend for the olefin binding on carbides of the group 6, as it depends on the crystal system of the bulk, the packing of atoms in the slabs, the geometry of the layers, and as a consequence, it also depends on the resulting electronic structure in every case.

The C_2H_4 binding could also be carried out through H atoms, i.e. if H atoms are directed towards the surface; however, it is among the less stable structures, which is a different behavior as reported for δ-MoC(001) surface.[30] Two binding modes through H atoms (H-down1 and H-down2, see Fig. S5) are possible on γ-WC(001) surface (see Table S2). However, on α-WC(0001) surface only H-down2 is possible while H-down1 is not, hence inducing a rotation of C–H axes to a plane close to that parallel to the surface (see Fig. S5). However, in any case the C=C bond is elongated when the binding is through H atoms.

The most stable adsorption structures on γ-WC(001) and α-WC-C surfaces involves the formation of a covalent $C_{ethylene}$–$C_{surface}$ bond, according to the CDD plots and ELF charts shown in Fig. 2, with the concomitant decrease in electron density in between the $C_{ethylene}$–$C_{ethylene}$ bond. In fact, the shared charge density between surface and ethylene is utilized in the formation of a covalent bond and, as a consequence, the adsorbed ethylene has a negligible net Bader charge (see Fig. 1). A different behavior is observed for C_2H_4 binding on α-WC-W, where the adsorbed ethylene received 1.1e from the surface, which is also observed in the CDD plot where the topmost layer loses electron density. Additionally, the CDD plot and the ELF chart indicates an increase in electron density in the region in between adsorbate and surface, which, together with the “charged” adsorbate, suggests both covalent and ionic contribution to the bonding in the ethylene-surface system. The

earned charge in adsorbed C_2H_4 is higher on α-WC-W (1.1e) than on Pt(111) (0.4e), which relates to the strength of the binding of ethylene on these surfaces.

At this point, it is worth to mention that the use of a sufficient amount of layers in a slab is very important since the results could have a different significance. Several tests were carried out to establish that a 6-layers slab size is appropriate to describe C_2H_4 binding on surfaces of tungsten carbides as mentioned above in the Methodology section. Here, we highlight that if a lower number of layers are used, e.g. 4-layers (keeping a constant 6% surface coverage), the results are completely different. This behavior is shown in Fig. S6 in the Supplementary Information, where if using the same initial adsorption geometry (in 4- and 6-layers slabs) then the results leads to different final structures., i.e. the structures are not converged using 4-layers slab. This particular behavior was observed mainly on the α-WC-W surface, while on α-WC-C and γ-WC(001) surfaces the geometries are similar by using 4- or 6-layers slabs, but the energy convergence was achieved only by using 6-layers slab. Therefore, the use of a certain number of layers should not be generalized, as it depends on the type of adsorbate. For comparison purposes, other adsorbates are contrasted. In the case of the H_2 dissociative chemisorption, using 4, 6, or 8 layers in a slab is equivalent in both geometry and energy aspects (see Table S1); however, it has been reported that for other adsorbates (CO, and CO_2)[38] a 4-layer slab is enough.

3.2. Characterization of ethylene adsorption on platinum and tugsten carbide surfaces

3.2.1. Vibrations of adsorbed ethylene

The vibrational modes corresponding to the gas phase C_2H_4 molecule could change due to the binding at the surface, which will depend on the binding strength and the adsorbed orientation. Therefore, the vibrations could serve as a fingerprint to characterize the behavior of C_2H_4 on tungsten carbide surfaces, providing and complementing information to experiments not available yet.

The predicted infrared spectra for the adsorbed ethylene are displayed in Fig. 3. The assignment of the vibrational modes are shown as sketches inside figure, and it is summarized in Table 2.

Though there are several reports about vibrations for C_2H_4 adsorbed on Pt(111), but to the best of our knowledge, we do not know reports regarding the DFT modelling of the vibrational modes and some specific assignments. In this work, we report the modelling of vibration modes and their respective spectra, for which some signals are in agreement to the range in wavenumbers for those reported experimentally[39–41] for the system C_2H_4–Pt(111), but here we also provide detailed assignments.

There is an intense peak at 441 cm^{-1} on Pt(111), which is assigned to a symmetric $C_{ethylene}$ upwards moving relative to the surface, with the motion of the C atoms but fixing the H atoms. This kind of vibration is also found in α-WC-W (397 cm^{-1}), where it belongs to

the most intense peak in that system. When the binding directly involves pure metal atoms in the topmost layer as on Pt(111) and α-WC-W surface, the intensity of the signal is high. On the contrary, if $C_{surface}$ atoms play a role as in the α-WC-C surface, the intensity is very low. Even though the γ-WC(001) surface has $C_{surface}$ and W atoms in every layer, where there are four W atoms surrounding every $C_{surface}$ atom in the *x*,*y* plane of the slab, a higher intensity was found at 335 cm^{-1}. This behavior indicates that the intensity of the signal at the lowest wavenumber is related to the amount of topmost surface metal atoms.

The symmetric $C_{surface}$–$C_{ethylene}$ stretching was observed at 1040 cm^{-1} and 907 cm^{-1} on α-WC-C and γ-WC(001), respectively. The charged surface composed of only $C_{surface}$ atoms in α-WC-C favors a stretching with the highest intensity, as expected due to favorable coupling between $C_{surface}$ and $C_{ethylene}$ atoms. Therefore, the ensemble effect in the topmost layer of γ-WC(001) affects the vibration extent of the $C_{surface}$–$C_{ethylene}$ system.

In a di-σ-CC binding mode, the $C_{surface}$ atoms also have a $C_{surface}$–$C_{surface}$ stretching, which was mainly observed in the γ-WC(001) system at 562 cm^{-1}. However, the stretching in the α-WC-C system is negligible. This behavior suggests that the α-WC-C system is less susceptible to surface distortion as compared to γ-WC(001), which is also in agreement with the trends discussed in section 3.3.

The adsorbed ethylene has a scissoring mode approaching H atoms to each other. This kind of vibration was predicted mainly in systems where surface metal atoms are exposed in the topmost layer. Therefore, the most intense signals were seen on Pt(111) and α-WC-W surfaces at 1416 cm^{-1} and 1409 cm^{-1}, respectively. The lower extent of W metal atoms exposed on γ-WC(001) leads to a decrease in the signal at 1427 cm^{-1}, while the absence of metal atoms exposed in the topmost layer of α-WC-C implies an absence of signal for that kind of vibration.

The trend for the C–H stretching was the same as for symmetric $C_{ethylene}$ upwards moving relative to the surface and the CH_2 scissoring mentioned above. Hence, the most intense peak was found on 3001 cm^{-1} on Pt(111), followed stretching on α-WC-W (3040 cm^{-1}), γ-WC(001) (2956 cm^{-1}), and α-WC-C (negligible).

The binding on α-WC-W has a characteristic small peak not found in other systems at 2446 cm^{-1}: a C–H stretching where H atoms are located atop W atoms. This could be useful to differentiate the C_2H_4 binding among different surfaces.

Overall, the stretching is highly influenced by the extent of surface metal atoms located in the topmost layer of the slab. This influences not only the intensity of the signal but a wavenumber shifting as well.

The infrared spectra and the associated peaks could serve as fingerprints to help to characterize the binding of ethylene on platinum and tungsten carbide surfaces, which could also be a bridge between modelling and future experiments.

3.2.2. Effect of ethylene binding on the electronic properties of surface and subsurface layers

The interactions of adsorbates on surfaces of solids reported in literature usually consider changes in the topmost layer of the slab; however, there is a lack of information about the role of sub-surface layers in the binding of several adsorbates, and no works have been reported in this way regarding C_2H_4 adsorption.

In this work, we analyze the role of both topmost and sub-surface layers in every 6-layers slabs of Pt(111), γ-WC(001), α-WC-C, and α-WC-W surfaces, which is characterized using PDOS and Bader charge analyses. Then, changes in the electronic structure of every layer in every system are analyzed before and after C_2H_4 binding, together with the establishment of Bader charges in every layer before ethylene binding and their changes due to the interaction with C_2H_4.

Overall, there is a general connection between adsorption energy and the extent of the changes in the electronic structure of the topmost layers of some slabs. Particularly, lower adsorption energies involves a major changes in the electronic structure as shown for the binding on γ-WC(001) and Pt(111) surfaces, as compared to the α-WC-C, and α-WC-W surfaces, where the adsorption energy is stronger which leads to a negligible changes in the electronic structure of the layers in the respective slabs (see Fig. 4). Even though the changes in the electronic structure mentioned above, there is always a charge reorganization leading to changes in the charge of the layers through the slab (from bulk to surface layers) favored by C_2H_4 binding as discussed below.

Details of changes in the electronic structure and Bader charges

Platinum

The adsorption on Pt(111) only affects the electronic structure of the first layer of the slab, as the PDOS of the *d*-orbitals changes (see Fig. 4a, layer 1), but the sublayer (layer 2) has no changes in the electronic structure due to the binding of C_2H_4. The PDOS for all the other layers of the slab has no changes relative to the clean surface (before adsorption); hence, there are no changes in the electronic structure in all the sublayers: from 2nd to 6th layer (see Fig. S7 in the Supplementary Information). Even though the electronic structure of the sublayers does not show modifications, there is a charge reorganization throughout the slab once C_2H_4 was adsorbed, as shown in the Bader charges for every slab before and after ethylene binding (see Table 3). The first layer lost 0.54e, which part of it is transferred into the ethylene, showing an earned charge of 0.4e in the adsorbed C_2H_4. This is an expected result for the first layer regarding the PDOS mentioned above (see Fig. 4a). However, different behavior is observed in all the sublayers, although there are no changes in the electronic structure before and after adsorption. The 3rd and 4th layers lost 0.23e and 0.61e, respectively, while the charges in the 5th layer increased by 0.54e, but the changes in the bottommost layer are negligible. Therefore, there is a charge reorganization from the 5th (4rd sub-layer) into the 1st layer (surface, topmost layer) of the slab, which indicates that sub-surface layers are participating of the binding but without modifying their electronic structure.

Tungsten carbide surfaces

A similar analysis was carried out for the adsorption on γ-WC(001), α-WC-C, and α-WC-W. In all the cases, there are changes in the PDOS of the first and/or second layer on the respective slabs, therefore only the PDOS of these layers are shown in Fig. 4. The complete PDOS, i.e. for the 6-layers slab in every surface, can be found in the Fig. S7-S11 of the Supplementary Information.

The main changes are observed for the binding on γ-WC(001) surface regarding the PDOS for *s,p*-orbitals in the 1st and 2nd layers, which is in agreement with the formation of a covalent $C_{surface}$–$C_{ethylene}$ bond according to the CDD plots (Fig. 2) discussed above. Small changes in the PDOS of the *d*-orbital are observed only for the 1st layer of γ-WC(001). This indicates that the charge loss of $C_{surface}$ atoms in direct contact with $C_{ethylene}$ is compensated by donation of charge from 5 neighbor W atoms (4 in *x,y* direction and 1 below in the 2nd layer) obeying the electronegativity difference between C (2.55) and W (2.36) atoms in the Pauli's scale. The compensation from a sub-surface W atom located in the 2nd layer is supported by a decrease of the *d*-orbitals PDOS at the Fermi level, indicating that the electronic structure is modified not only in the surface but in the first layer of the sub-surface for the binding on γ-WC(001). The changes in the Bader charge was observed from the 1st layer (surface, topmost layer) until the 3rd layer (2nd sub-surface layer), while there are negligible changes in the 4th, 5th, and 6th layers. Therefore, the binding on γ-WC(001) only affects the topmost 3 layers of the slab. In the 1st layer, there is a decrease in the Bader charge of 1.93e, which is related with the "use" of electron density in the formation of two $C_{surface}$–$C_{ethylene}$ bonds, and the charge transfer towards sub-layers, since ethylene also provides electron density which migrates until the 3rd layer, leading to an increase of Bader charges for the 2nd (0.72e) and 3rd (0.88) layers. However, the electron donation-back donation between adsorbate and surface leads to the formation of a covalent $C_{surface}$–$C_{ethylene}$ bond, which induces a negligible net charge in the adsorbed ethylene (see Fig. 1).

The PDOS of α-WC-C and α-WC-W due to C_2H_4 adsorption is only slightly affected in the *d*-orbitals. In the case of α-WC-C, the PDOS of orbitals *s,p* for topmost layer composed of C atoms is not modified, however, the sub-surface layer composed of W atoms share electron density with the C surface layer to compensate for the loss of used charge in the formation of two $C_{surface}$–$C_{ethylene}$ bonds, which is also seen in a decrease of Bader charge (6.26e) in the W sub-layer. In the α-WC-W system, only the topmost layer of W atoms has changed the electronic structure, while the sub-layer of C atoms does not have significant changes. However, the C_2H_4 binding involves charge transfer from the 1st to the 4th layer in α-WC-C, while a transfer from the 1st to the 5th layer in α-WC-W. The topmost layer of W in α-WC-W lost charge (1.06e), while the sub-surface C layer earned charge (1.41), which indicates that the charge transferred from W topmost layer into the ethylene (to yield 1.1 in the adsorbate, see Fig. 1) is not compensated by the sub-surface C layer; instead of that, some charge of W topmost layer could be transferred towards the C sub-layer. Therefore, the C sub-layer acts as a bridge between other sub-surface layers and the system atop it, i.e. W topmost surface and ethylene.

A general trend is observed at this point: if the topmost layer is composed of only metal atoms, the charge reorganization is inducing changes from the 4th sub-layer, but for surfaces containing C atoms in the topmost layer, the charge reorganization (changes) is from the 3rd or 2nd sublayer into the topmost layer.

Hence, 2, 3, and 4 sub-surface layers play a key role in the binding of ethylene on γ-WC(001) and α-WC-C and α-WC-W surfaces, respectively, since they provide electron density into the surface and the adsorbate, in other words, there is a charge reorganization leading to shifings in the charge of the layers from the bottom layers into the surface, favored by the interaction with the adsorbate.

3.3. Geometric activation of the ethylene C=C bond and surface distortion

Geometric activation

The C_2H_4 molecule is activated on all the evaluated surfaces, since there is an elongation of the ethylene C–C bond length (see Table 1) from 1.33 Å (free ethylene) to a distance close or slightly above to 1.53 Å (free ethane, desired product in C_2H_4 hydrogenation).

The extent of the elongation for the $C_{ethylene}$–$C_{ethylene}$ bond length is more significant when $C_{surface}$ atoms are directly involved in binding the adsorbate, i.e. on γ-WC(001) and α-WC-C surfaces (di-σ-CC mode), with an elongation of 0.27 Å in both cases. The binding on surface metal sites involves a $C_{ethylene}$–$C_{ethylene}$ elongation of 0.16 Å on both Pt(111) and α-WC-W surfaces.

Though the C=C activation is observed for the most stable mode in every case, the C=C was also activated in other less stable cases (see Tables S2 and S3). On the γ-WC(001) surface, C_2H_4 was activated on the bridges $C_{surface}$-W (di-σ-CM) and W-W (di-σ-MM), in addition to an adsorption in π-C mode, which was also observed on α-WC-C where it is the less stable structure. Therefore, the preference is to activate C=C bond by using two surface sites (C and/or W) instead of only one $C_{surface}$ site. The binding of ethylene on α-WC-W has not a "pure" surface sites as seen for the other surfaces discussed above, but it has a hybrid surface site composed with five surface W and two sub-surface C atoms.

Surface distortion

The binding of ethylene could cause a surface distortion, depending on the involved sites in the adsorption process. Particularly, the surface distortion is more significant when the binding is via a di-σ-CC mode as observed on γ-WC(001) and α-WC-C surfaces (Fig. 1), which is shown in Fig. 5. In these cases, once the $C_{ethylene}$ atoms are approached to the surface, there is a slight upwards shifting of $C_{surface}$ atoms to favor an orbital overlap to form the $C_{ethylene}$–$C_{surface}$ covalent bond. The upwards shifting after adsorption of the $C_{surface}$ atoms involved in the binding is 0.61 Å and 0.15 Å for γ-WC(001) and α-WC-C surfaces, respectively, which relates to the surface distortion energy extent shown in Fig.

5. If C_2H_4 binding involves a charged layer of W atoms (α-WC-W), the surface distortion is negligible (0.05 eV and 0.01 Å), while the binding on Pt(111) induces an upwards shifting of 0.13 Å of Pt atoms involved in the binding. Therefore, the presence of a sub-surface composed only of C atoms in α-WC-W surface stabilizes the topmost layer avoiding surface relaxation, an opposite behavior as observed in Pt(111), γ-WC(001), and α-WC-C, where the absence of a charged carbon sub-surface layer favors a surface relaxation due to C_2H_4 binding.

The calculated energies reported in Table 1 were also obtained considering a ZPE term. The highest ZPE term is observed for the binding on γ-WC(001) and α-WC-C surfaces, which relates to the high surface distortion of these surfaces as compared to Pt(111) and α-WC-W (ZPE term in both cases is negligible, see Table 1). Therefore, the larger the surface distortion the higher ZPE term. This could also be due to the inclusion of $C_{surface}$ atoms in the coupling with $C_{ethylene}$ atoms, which was not considered when metal atoms are involved in the binding, as the coupling between C and M atoms is negligible. Even though the ZPE term for the absolute energy (surface+ethylene system) is low in all the cases (< 0.23%), it has a remarkable effect in the adsorption energy as well (0.6% to 36.8%). Therefore, a ZPE term should always be considered if the binding of ethylene involves $C_{surface}$ atoms to better account for the comprised energies in the C_2H_4 adsorption, which could be useful in further studies regarding ethylene hydrogenation.

General trends of ethylene activation on transition metal carbide surfaces

The ethylene molecule can be activated on several surfaces of different transition metal carbides, which also have a variety of surface sites in terms of geometry and bonding properties. Therefore, the characterization of the C–C elongation requires an additional correlation to better account general information regarding C_2H_4 activation. Therefore, we propose a relation of adsorption energy (DFT+vdW) and C–C elongation length, as shown in Fig. 6, where general trends can be achieved. The information in Fig. 6 comprises not only the tungsten carbide surfaces discussed above, but also ethylene binding on Pt(111), δ-MoC(001), TiC(001), ZrC(001), β-Mo_2C-C, and β-Mo_2C-Mo surfaces as reported previously.[30,31] Overall, the activation of the C=C bond could be grouped into three sets: group I, II, and III.

Group I: The ethylene is adsorbed but is not activated, as there is not a change in the geometry of the adsorbate, i.e. C=C bond length and a sp^2 hybridization remain the same for C_2H_4 as in the gas phase. Particularly, this behavior was observed for the π-M adsorption mode in all the evaluated surfaces, i.e. when only one surface metal atom is directly involved in the binding.

Group II: The C_2H_4 is activated, i.e. there is an elongation of C–C bond, together with C–H bond length elongations and a modification of the hybridization from sp^2 to sp^3-like. In this group, there are five kinds of surface sites and adsorption modes to activate C_2H_4: 1) π-C, 2) σ-C, 3) di-σ-CM, 3) di-σ-MM, and 4) hybrid. In the π-C and σ-C modes, only one $C_{surface}$ atom is the main responsible of the binding and activation, while in the other modes two or more surface atoms are directly involved. Particularly, in di-σ-CM ($C_{surface}$–

Metal bridge) and di-σ-MM (M–M bridge) modes two surface atoms are responsible of the activation, while in surfaces like β-Mo_2C-C, β-Mo_2C-Mo, and α-WC-W, more than two surface atoms actively participate in the activation; hence they are named as hybrid sites. The range of C–C elongation is from 1.43 Å to 1.55 Å, whose values are close to the C–C bond length of free ethane (1.53 Å), the desired product in C_2H_4 hydrogenation.

Group III: A similar behavior is observed as in *Group II*. The difference is the larger extent of the ethylene C–C bond length elongation in the range 1.60 – 1.64 Å, which is above the C–C bond length value of free C_2H_6. This behavior was only observed when two $C_{surface}$ atoms are bonded with ethylene in a di-σ-CC adsorption mode as shown in Fig. 1 b, c, but the same applies to TiC(001) as reported[30] previously. The extent of the ethylene C–C elongation could have implications in the catalytic application of the metal carbides not only in hydrogenation but in hydrogenolysis reactions. However, the energy barriers involved in these reactions could answer those questions, which deserves studies out of the scope of the current work that could be a matter of future work.

The results in Fig. 6 suggest that the ethylene C=C geometric activation takes place on only certain surface sites and adsorption modes, where the obtained adsorption energy and ethylene C-C bond length elongation leads to only 3 groups to classify the activation. These results could be extrapolated to other systems, particularly transition metal carbides and their interaction with olefins in general.

4. Summary and Conclusions

We have performed the first systematic study for the adsorption and activation of an olefin on tungsten carbide surfaces. The bonding of the molecule is far from being trivial, and strongly depends on the orientation and termination of the carbide surface.

The most stable structure on γ-WC(001) and α-WC-C surfaces has a di-σ-CC mode, while the binding on α-WC-W implies hybrid surface sites. The binding energy extent follows the trend: α-WC-C (-3.35 eV) > α-WC-W (-2.24 eV) > Pt(111) (-1.78 eV) > γ-WC(001) (-1.19 eV), where the C_2H_4 was activated, i.e. an elongation of the C–C bond length was observed together with changes of sp^2 into sp^3-like hybridization.

The results for the elongation of the C–C bond obtained in this work were compared with previous studies with other transition metal carbides surfaces, leading to a general classification of the C–C bond elongation into three sets: *group I*, *group II*, and *group III*. Every group has some particular surface sites and binding modes, together with the relationship to adsorption energies. Hence, if the interest is to activate ethylene C=C bond, the surface sites and the binding modes should be those of the groups II and III.

The effect in the geometry and electronic structure of the surface due to C_2H_4 adsorption were also analyzed. The results indicate that only the topmost layers can be susceptible to modify their electronic structure, but the sub-surface layers are also participating in the binding without modifying their electronic structure. In other words, there is a charge

reorganization from the bulk into the topmost surface at long ranges (above 6 Å). Regarding the geometric changes, there is a larger surface distortion if ethylene binding involves carbon surface atoms, like on γ-WC(001) and α-WC-C surfaces where the binding was via di-σ-CC mode, favoring an upward shift of $C_{surface}$ atoms of 0.61 Å and 0.15 Å, respectively. However, the surface distortion when binding was carried out on metal sites is negligible. The surface distortion relates to the ZPE term to the electronic energy established for the evaluated systems.

The vibrational spectra for all the studied systems were simulated. Overall, there are four signals accounting for different vibration modes. This data could serve as a bridge for further experiments and/or theoretical studies.

The results of this work indicate that there is a preference for ethylene to bind on α-WC-C (-2.91 eV), which could eventually induce surface poisoning. On the contrary, the binding on α-WC-C is weaker (-1.68), indicating that this surface could be the most relevant in catalysis, where further kinetic studies should be addressed to support this hypothesis. In this way, the results for the metastable γ-WC(001) system are promising (-0.72 eV). However, an experimental challenge arises in the way to synthesize this phase preferentially together with enough lifetime to allow its application as a catalyst.

The results of the current work open a window to further studies regarding the mechanism of ethylene hydrogenation on these still unexplored surfaces for hydrogenation of olefins and other complex unsaturated hydrocarbons.

5. Acknowledgements

Part of this research was carried out at the University of Sydney. Particularly the Raijin facility of the Australian National Computational Initiative was used. Part of this research used resources of the Center for Functional Nanomaterials, which is a U.S. DOE Office of Science Facility, and the Scientific Data and Computing Center, a component of the Computational Science Initiative, at Brookhaven National Laboratory under Contract No. DE-SC0012704. C J-O and E F acknowledge to Universidad de Medellín for financial support. The authors acknowledge to Francesc Viñes, who developed and provided a script for calculating vibrational frequencies in periodic systems applied to the VASP code.

6. Conflicts of interest

The authors declare no conflicts of interest.

7. References

1 R. . Levy and M. Boudart, *Science*, 1973, **181**, 547–549.

2 I. Kojima, E. Miyakasi, I. Yasunobu and I. Yasumori, *J. Catal.*, 1979, **59**, 472–474.

3 I. Kojima, E. Miyakasi, I. Yasunobu and I. Yasumori, *J. Catal.*, 1982, **73**, 128–135.

4 W. Xu, P. J. Ramirez, D. Stacchiola and J. A. Rodriguez, *Catal. Letters*, 2014, **144**, 1418–1424.

5 P. Liu and J. A. Rodriguez, *J. Phys. Chem. B*, 2006, **110**, 19418–19425.

6 S. J. Ardakani and K. J. Smith, *Appl. Catal. A Gen.*, 2011, **403**, 36–47.

7 S. J. Ardakani, X. Liu and K. J. Smith, *Appl. Catal. A Gen.*, 2007, **324**, 9–19.

8 B. Dhandapani, T. St. Clair and S. T. Oyama, *Appl. Catal. A Gen.*, 1998, **168**, 219–228.

9 G. Vitale, H. Guzmán, M. L. Frauwallner, C. E. Scott and P. Pereira-Almao, *Catal. Today*, 2015, **250**, 123–133.

10 X. Liu, A. Tkalych, B. Zhou, A. M. Köster and D. R. Salahub, *J. Phys. Chem. C*, 2013, **117**, 7069–7080.

11 H. H. Hwu and J. G. Chen, *Chem. Rev.*, 2005, **105**, 185–212.

12 G. Vértes, G. Horányi and S. Szakács, *J. Chem. Soc., Perkin Trans. 2*, 1973, 1400–1402.

13 A. S. Rocha, A. B. Rocha and V. T. da Silva, *Appl. Catal. A Gen.*, 2010, **379**, 54–60.

14 J. Brillo, R. Sur, H. Kuhlenbeck and H.-J. Freund, *J. Electron Spectros. Relat. Phenomena*, 1998, **88–91**, 809–815.

15 J. Brillo, A. Hammoudeh, H. Kuhlenbeck, N. Panagiotides, S. Schwegmann, H. Over and H.-J. Freund, *J. Electron Spectros. Relat. Phenomena*, 1998, **96**, 53–60.

16 C. Moreno-Castilla, M. A. Alvarez-Merino, F. Carrasco-Marín and J. L. G. Fierro, *Langmuir*, 2001, **17**, 1752–1756.

17 J. Lemaitre, V. Benoit and L. Leclercq, *J. Catal.*, 1986, **99**, 415–427.

18 A. S. Kurlov and A. I. Gusev, in *Tungsten Carbides. Structure, Properties and Application in Hardmetals*, Springer International Publishing, 1st edn., 2013, pp. 5–56.

19 A. Y. Liu and M. L. Cohen, *Solid State Commun.*, 1988, **67**, 907–910.

20 A. Antoni-Zdziobek, J. Y. Shen and M. Durand-Charre, *Int. J. Refract. Met. Hard Mater.*, 2008, **26**, 372–382.

21 F. Viñes, C. Sousa, P. Liu, J. A. Rodriguez and F. Illas, *J. Chem. Phys.*, 2005, **122**, 174709.

22 Y.-J. Tong, S.-Y. Wu and H.-T. Chen, *Appl. Surf. Sci.*, 2018, **428**, 579–585.

23 X. Zhang, Z. Yang and R. Wu, *Nanoscale*, 2018, **10**, 4753–4760.

24 X. Zhang, Z. Lu and Z. Yang, *Appl. Surf. Sci.*, 2016, **389**, 455–461.

25 Y. Liang, L. Chen and C. Ma, *Surf. Sci.*, 2017, **656**, 7–16.

26 Y. Xi, L. Huang, R. C. Forrey and H. Cheng, *RSC Adv.*, 2014, **4**, 39912.

27 W. Zheng, L. Chen and C. Ma, *Comput. Theor. Chem.*, 2014, **1039**, 75–80.

28 D. D. Vasić, I. A. Pašti and S. V. Mentus, *Int. J. Hydrogen Energy*, 2013, **38**, 5009–5018.

29 D. D. Vasić Anićijević, V. M. Nikolić, M. P. Marčeta-Kaninski and I. A. Pašti, *Int. J. Hydrogen Energy*, 2013, **38**, 16071–16079.

30 C. Jimenez-Orozco, E. Florez, A. Moreno, P. Liu and J. A. Rodriguez, *J. Phys. Chem. C*, 2016, **120**, 13531–13540.

31 C. Jimenez-Orozco, E. Florez, A. Moreno, P. Liu and J. A. Rodriguez, *J. Phys. Chem. C*, 2017, **121**, 19786–19795.

32 G. Kresse and J. Furthmüller, *Phys. Rev. B*, 1996, **54**, 11169–11186.

33 G. Kresse and D. Joubert, *Phys. Rev. B*, 1999, **59**, 1758–1775.

34 H. J. Monkhorst and J. D. Pack, *Phys. Rev. B*, 1976, **13**, 5188–5192.

35 G. Henkelman, A. Arnaldsson and H. Jónsson, *Comput. Mater. Sci.*, 2006, **36**, 354–360.

36 W. Tang, E. Sanville and G. Henkelman, *J. Phys. Condens. Matter*, 2009, **21**, 084204.

37 E. Sanville, S. D. Kenny, R. Smith and G. Henkelman, *J. Comput. Chem.*, 2007, **28**, 899–908.

38 A. A. Koverga, E. Flórez, L. Dorkis and J. A. Rodriguez, *J. Phys. Chem. C*, 2019, **123**, 8871–8883.

39 P. S. Cremer, X. C. Su, Y. R. Shen and G. a Somorjai, *J. Am. Chem. Soc.*, 1996, **118**, 2942–2949.

40 P. S. Cremer and G. A. Somorjai, *J. Chem. Soc. Faraday Trans.*, 1995, **91**, 3671.

41 A. Tillekaratne, J. P. Simonovis and F. Zaera, *Surf. Sci.*, 2016, **652**, 134–141.

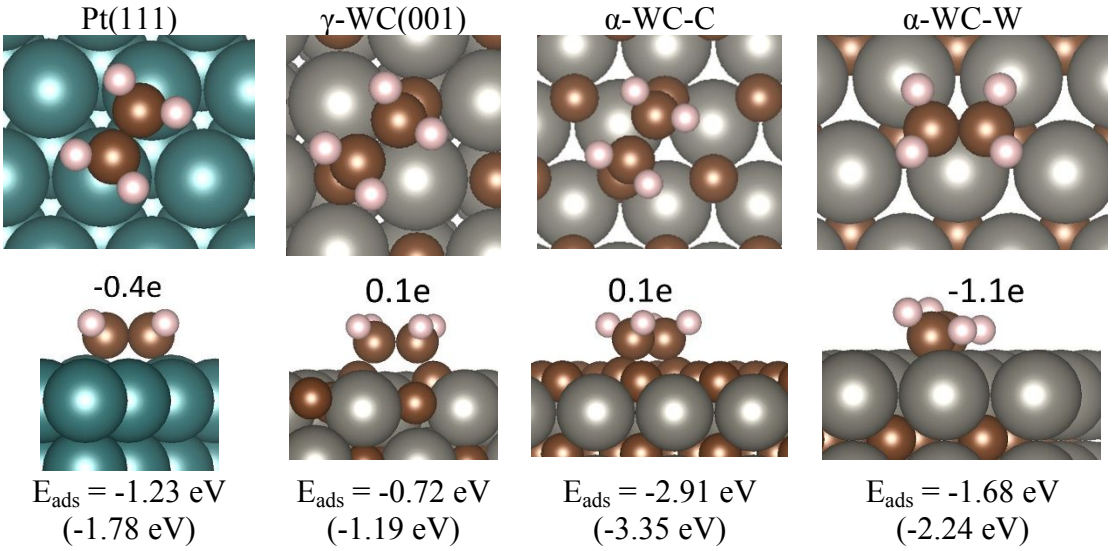

Fig. 1. Most stable adsorption modes on Pt(111), γ-WC(001), α-WC-C, and α-WC-W surfaces. Top and side views. The Bader charge for the adsorbed molecule is shown. The values in parenthesis indicate to the DFT+vdW adsorption energy. Pt, C, W, and H atoms are represented by turquoise, brown, dark gray, and light gray colors, respectively.

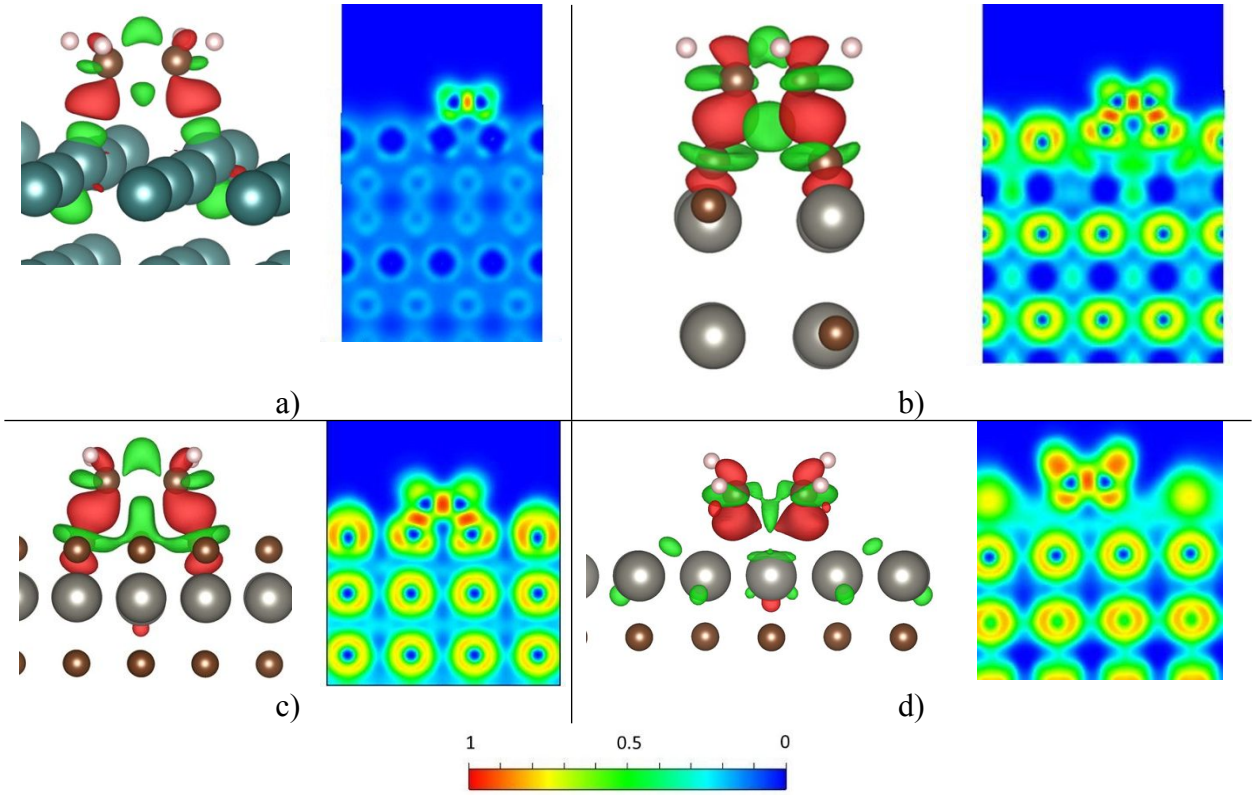

Fig. 2. CDD (iso-surfaces of 0.01 eV/Å^3) and ELF for: a) Pt(111), b) γ-WC(001), c) α-WC-C, d) α-WC-W. Red and green regions in CDD represent earned and lost electron density.

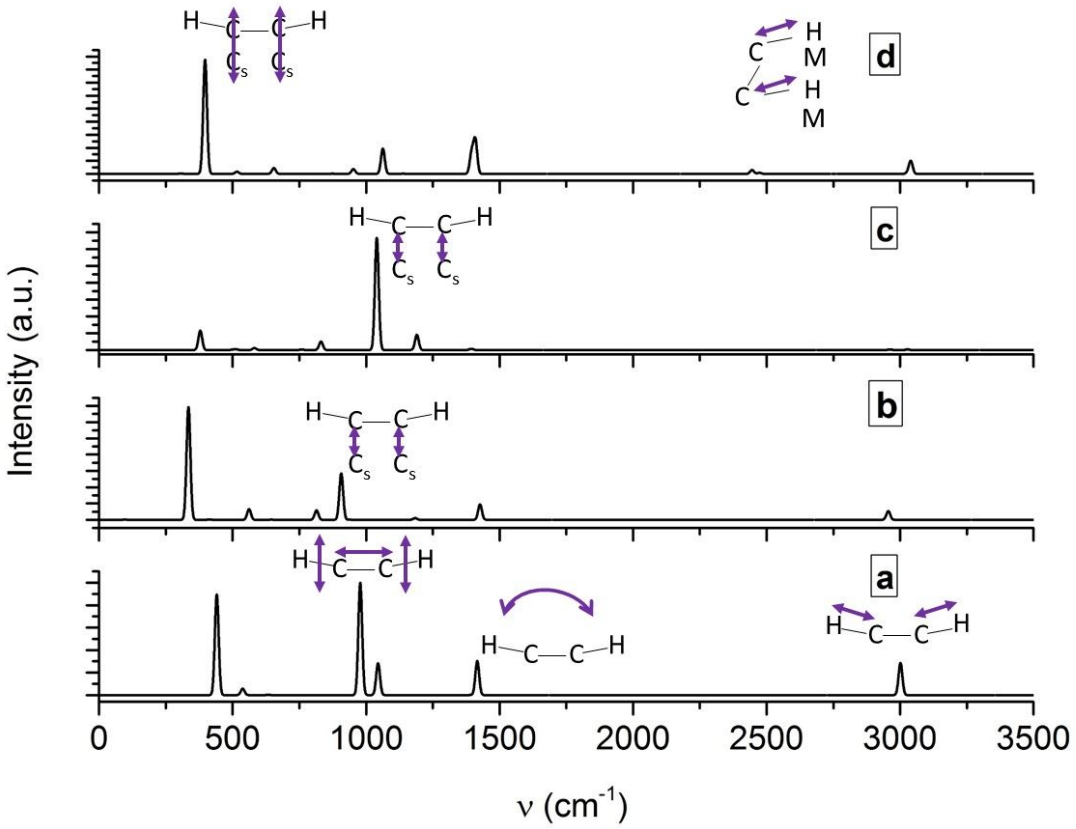

Fig. 3. Infrared spectra for adsorbed C_2H_4 on: a) Pt(111), b) γ-WC(001), c) α-WC-C, and d) α-WC-W surfaces.

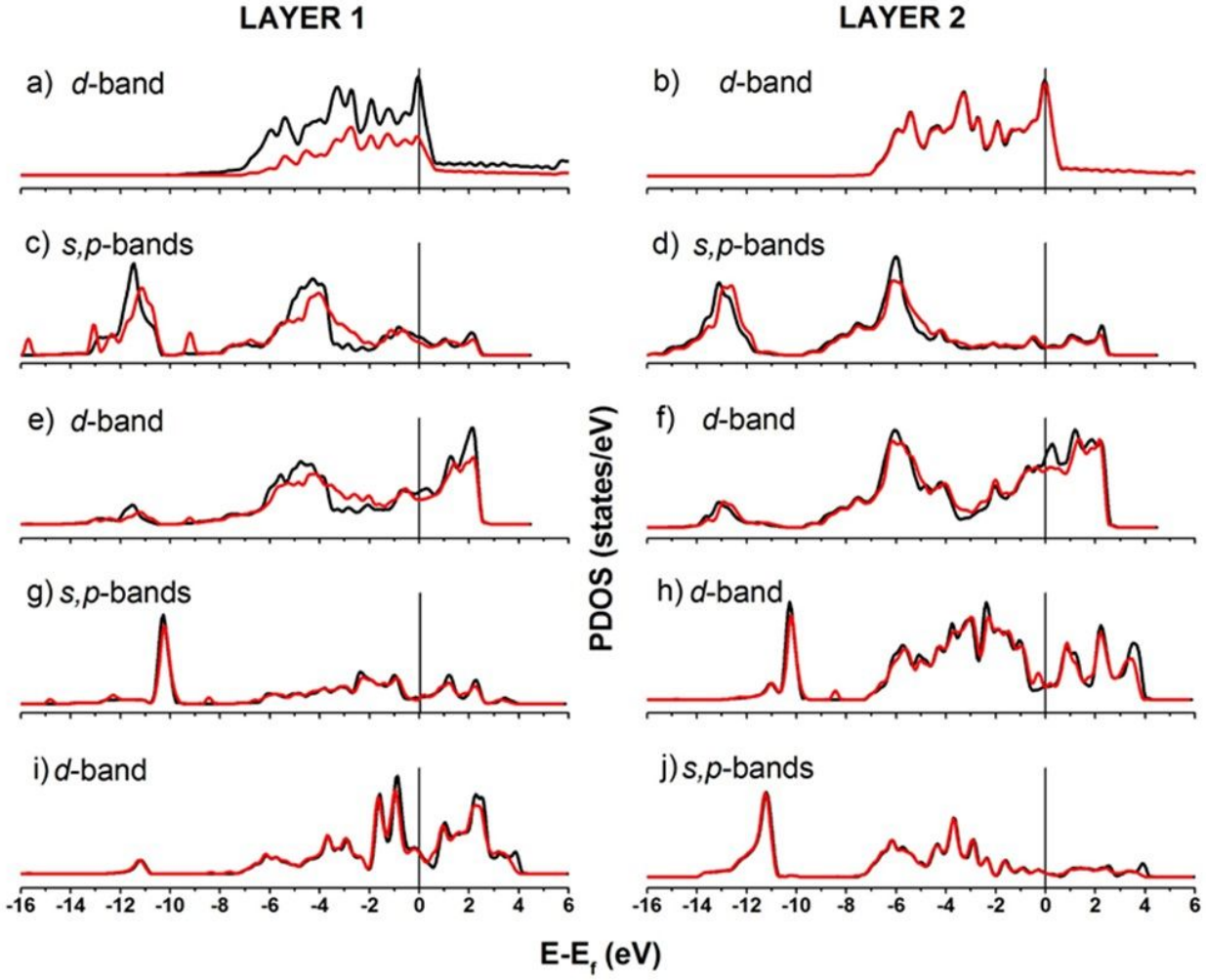

Fig. 4. PDOS for the topmost two layers in the respective surface slab: layer 1= topmost, layer 2 = first sublayer. Black and red lines represent the PDOS before and after ethylene adsorption, respectively. The vertical line in every case indicates the Fermi level. Pt(111): a), b); γ-WC(001): c)-f); α-WC-C: g), h); α-WC-W: i), j).

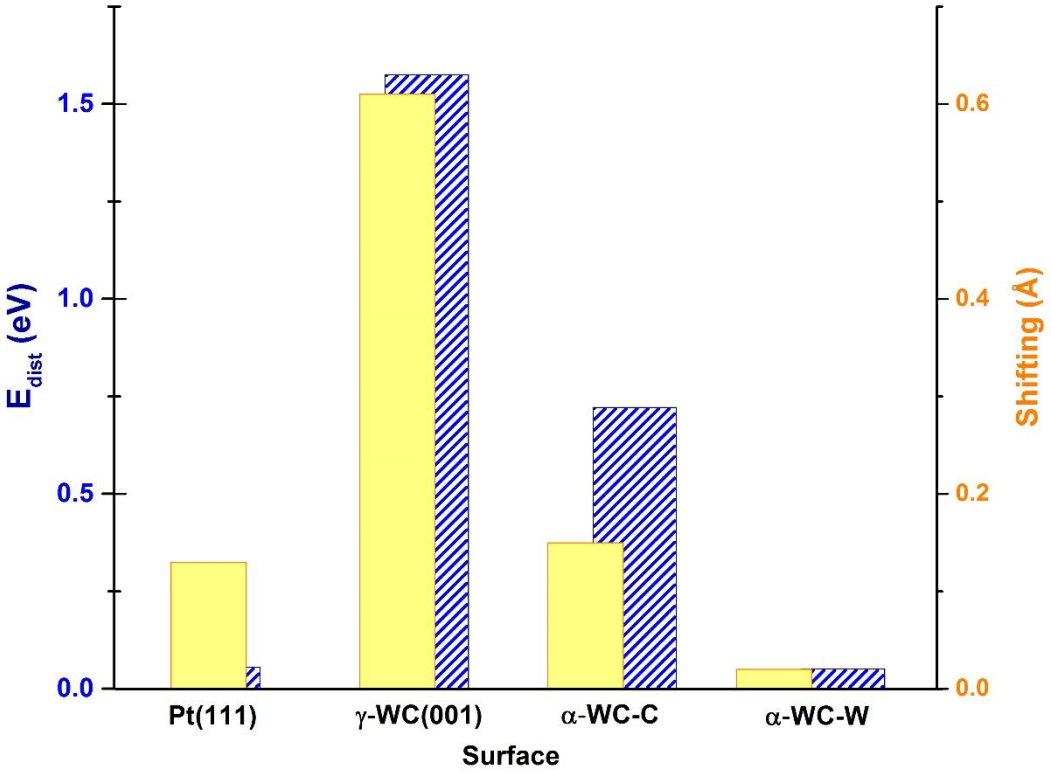

Fig. 5. Surface distortion energy (E_{dist}) and surface atom upwards shifting caused by C_2H_4 adsorption.

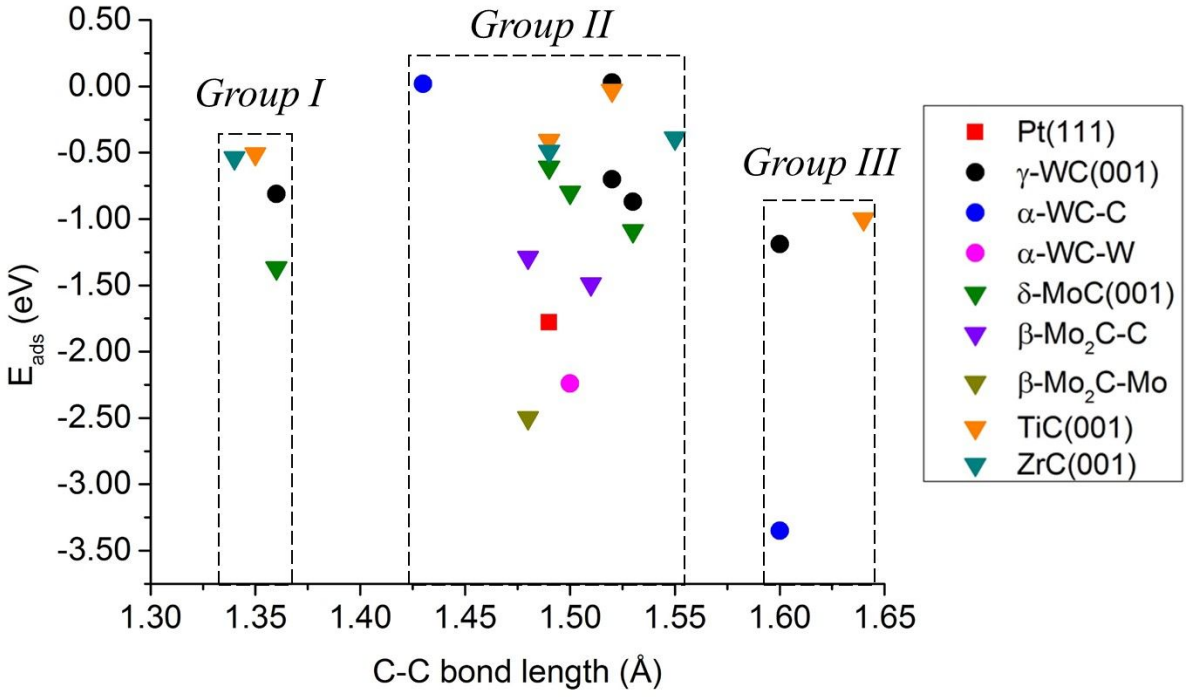

Fig. 6. Classification of the elongation of ethylene C–C bond on several surfaces of transition metal carbides and Pt(111).

Table 1. Most stable adsorption modes (DFT and DFT+vdW, Eq. 1) for ethylene binding on Pt(111), γ-WC(001), and α-WC(0001) surfaces. C-C bond elongations and ZPE term (Eq. 2) are included.

Surface	Mode	DFT (eV)	DFT+vdW (eV)	% vdW	C-C[a] (Å)	% ZPE ($E_{absolute}$)	% ZPE ($E_{adsorption}$)
Pt(111)	di-σ-MM	-1.23	-1.78	30.5	1.49	0.22	3.8
γ-WC(001)	di-σ-CC	-0.72	-1.19	39.8	1.60	0.15	36.8
α-WC-C	di-σ-CC	-2.91	-3.35	13.3	1.60	0.16	12.3
α-WC-W	C-H, C-H	-1.68	-2.24	24.9	1.50	0.13	0.6

[a] C=C bond length of free ethylene is 1.33 Å.

Table 2. Assignment of vibration frequencies to the wavenumbers for the adsorbed ethylene. The most intense peak in every case is highlighted.

Pt(111)	
ν (cm^{-1})	**Assignment**
441	wagging (C-C)
538	$\nu_{assymetric}$ (C-C), CH_2 out of plane
978	ν_s (C-C)
1045	ν_s (C-C), CH_2 bending
1416	CH_2 bending out of plane
3001	ν_s (C-H_2)
γ-WC(001)	
335	$C_{surface}$,up
562	ν_s ($C_{surface}$-$C_{surface}$)
814	ν_s ($C_{ethylene}$-$C_{ethylene}$), $C_{surface}$,up
907	ν_s ($C_{ethylene}$-$C_{surface}$)
1427	CH_2 bending: wagging
2956	ν_s (C-H_2)
α-WC-C	
379	$C_{surface}$,up
831	ν_s ($C_{ethylene}$-$C_{ethylene}$), $C_{surface}$,up
1040	ν_s ($C_{ethylene}$-$C_{surface}$)
1190	CH_2 bend: wagging
α-WC-W	
397	$C_{surface}$,up
1063	CH_2 bend: wagging
1409	CH_2 bend: scissors
2446	$\nu_{assymetric}$ (C-H)
3040	ν_s (C-H)

Table 3. Net Bader charge (*e* units) in every layer of the respective slab before and after ethylene adsorption; Δρ indicates the charge change in every case.

Layer	After	Before	Δρ
Pt(111)			
1	-0.77	-0.23	-0.54
2	0.77	-0.48	1.25
3	0.12	0.35	-0.23
4	0.81	1.42	-0.61
5	-0.65	-1.19	0.54
6	0.10	0.12	-0.02
γ-WC(001)			
1	-0.24	1.69	-1.93
2	-0.78	-1.50	0.72
3	1.10	0.22	0.88
4	-0.36	-0.33	-0.03
5	0.14	-0.01	0.15
6	0.09	-0.05	0.14
α-WC-C			
1	-10.89	-14.68	3.79
2	19.92	26.18	-6.26
3	-21.38	-23.22	1.84
4	23.58	23.13	0.45
5	-22.97	-22.97	0.00
6	11.68	11.57	0.11
α-WC-W			
1	10.19	11.25	-1.06
2	-17.90	-19.31	1.41
3	18.15	17.66	0.49
4	-17.24	-16.89	-0.35
5	14.60	13.93	0.67
6	-6.68	-6.63	-0.05

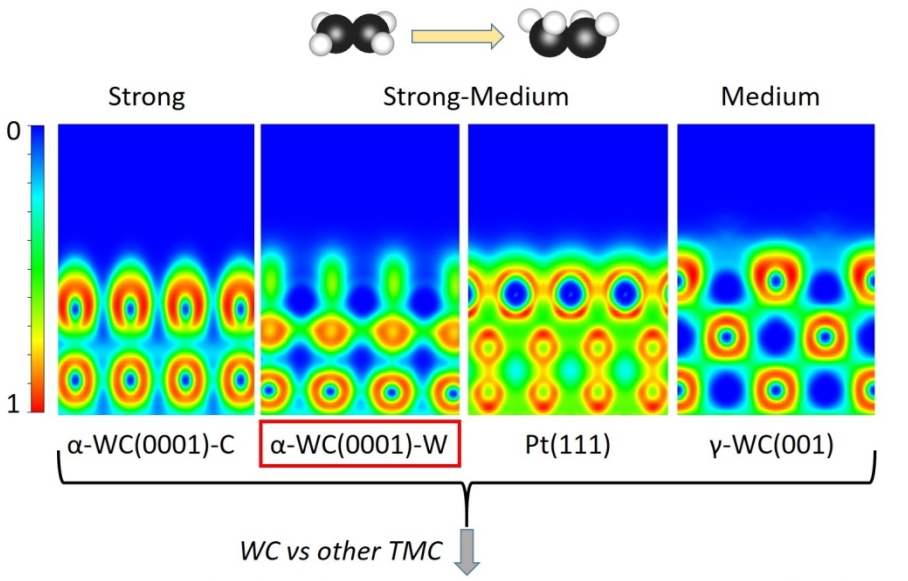

General classification of ethylene activation on transition metal carbides

289x182mm (150 x 150 DPI)